Journal of Advanced Research in Geo Sciences & Remote Sensing
Volume 7, Issue 3&4 - 2020, Pg. No. 1-20
Peer Reviewed Journal

Research Article

Significance of the Geochemistry, Petrogenesis and Tectonic Evolution of the Neoproterozoic Amphibolites groups within the Gneisses and Migmatites from El Obeid Area, North Kordofan State, Sudan

Hassan A Mustafa[1], Mushal A Salih[1], Asim A Elmansour[1], Mohammed I Abdelsamad[1], Mohammed A Elhadi[3], Einas M Slama[1,2]

[1]Faculty of Science, University of Kordofan, El Obeid, P.O 160, Sudan.
[2]Faculty of Earth Science, China University of Geosciences, Wuhan, 430074, China.
[3]Faculty of Science, University of Aljazeera, Wad Madani, Sudan.

I N F O

Corresponding Author:
Hassan A Mustafa, Faculty of Science, University of Kordofan, El Obeid, P.O. 160, Sudan.
E-mail Id:
ham3019@yahoo.com
How to cite this article:
Mustafa HA, Salih MA, Elmansour AA. Significance of the Geochemistry, Petrogenesis and Tectonic Evolution of the Neoproterozoic Amphibolites groups within the Gneisses and Migmatites from El Obeid Area, North Kordofan State, Sudan. *J Adv Res Geo Sci Rem Sens* 2020; 7(3&4): 1-20.

Date of Submission: 2020-08-05
Date of Acceptance: 2020-10-13

A B S T R A C T

El Obeid area consists of a suite of ~1.0 Ga amphibolites that are associated with the gneisses & migmatites. Petrographic and geochemical analyses of these amphibolites indicated that they correspond to basalts that derive from sub-alkaline magmas; and they classified into two groups. Group A which is cropped out in J. El Eiza'a suffered from weakly anatexis of the first metamorphic event and characterized by low Nb contents (0.44–0.96 ppm), and REE and multi-elemental patterns similar to N-MORB. Group B amphibolites within the gneisses and migmatites in J. Kordofan, only undergone the second metamorphic processes and has high Nb contents ranging from 2.00 to 18.7 ppm, displaying an E-MORB and Pickle Nb-enriched basalt geochemical signature. The low silica and MgO concentrations for the two groups respectively (SiO_2= 47.8–49.3 and 46.7–50.7 wt %) and (4.40–6.44 and 5.69–7.91%), suggested a mantle source for both groups. Their variable values of La/Ta (15.6–20.3 and 9.20–22.8), La/Nb (1.19–1.96 and 0.91–2.59) and Ba/Nb ratios (13.9–51.9 and 0.70–5.02), respectively, suggesting that they were likely derived from an average melt modified sub-continental lithospheric mantle, also their completely different REE profiles indicated authenticated their heterogeneous mantle source. Both groups have an arc-like and back-arc settings and show inputs of newly subduction-derived melt in the wedge source. Regional relationships indicated that the formation of these rocks resulted from the episodic amalgamation event during that time, an exterior accretion orogeny along the margin of Rodinia during ~1.0 Ga.

Keywords: Amphibolites, Geochemistry, Kordofan, Sub-alkaline, Rodinia

Introduction

The earth had been built from multiple movements of major or super cratons forming supercontinents through the geological time. The supercontinents block the heat flow from the Earth's interior, which represent the asthenosphere mantle. Eventually, the lithosphere begins to dome upward and breaks these supercontinents. Hot debates on how these supercontinents re-joined after separation, or they moved apart and then joined again, which carry up to the assembly-breakup of the supercontinents from the movements of the plate tectonics by convergence (subduction, accretion, collision) and divergence (rifting and breakup).

The general view for the first supercontinents reconstructions started with the assembly of the older plates during the Neoarchean ~2.7 Ga to form Kenorland one of the earliest supercontinents (Williams et al. 1991; Reddy and Evans, 2009) through series of accretion events (Halla, 2005; Geofrik, 2013). During the early Paleoproterozoic time numerous large igneous activities including the global pulse ~2.45 Ga in response to Kenorland breakup (Heaman, 1997) lasted by the presence of mafic dikes, river drift and sedimentary rift margins in many current continents. The Paleoproterozoic period witnessed the breakup of the supercontinent Kenorland and assembly and breakup of the supercontinent Columbia (Figure 1).

The Columbia supercontinent that existed in the Paleoproterozoic –Mesoproterozoic consists of proto-cratons that made up the former continents of Laurentia, Baltica, Ukrainian Shield, Amazonia, Australia, Siberia, North China and Kalaharia. The first assemblage of Columbia considered during 2.2–1.8 Ga (Rogers, 1996; Hoffman, 1997; Meert, 2002, 2012; Rogers and Santosh, 2002, 2003; Bleeker, 2003; Zhao et al., 2002c, 2004; Roberts, 2013; Nance et al., 2014). The collisional events that represent the assembly of Columbia supercontinent during that time in South America , West Africa, North America, Greenland, Baltica, Siberia, South Africa, in Western Australia, and ogen in North China (Zhao et al., 2002a, 2004, 2011). This supercontinent underwent long-lived continental marginal subduction-related accretion during 1.8–1.3 Ga. Columbia supercontinent breakup began at ~1.6 Ga, forming many continental rift zones along the western margin of Laurentia, southern margin of Baltica, southeastern margin of Siberia, northwestern margin of South Africa, and northern margin of North China. Also the break-up of Columbia associated with widespread magmatic activities in the western margin of Laurentia, eastern India, southern margin of Baltica, southeastern margin of Siberia, northwestern margin of South Africa, and northern margin of the North China Craton. The magmatic activity continued until the final breakup of the supercontinent at ~ 1.3-1.25 Ga, as recorded from the emplacement of the 1.27 Ga Mackenzie and 1.24 Ga Sudbury, Seal Lake, Harp, and Mealy mafic dike swarms in North America (Zhao, et al., 2011).

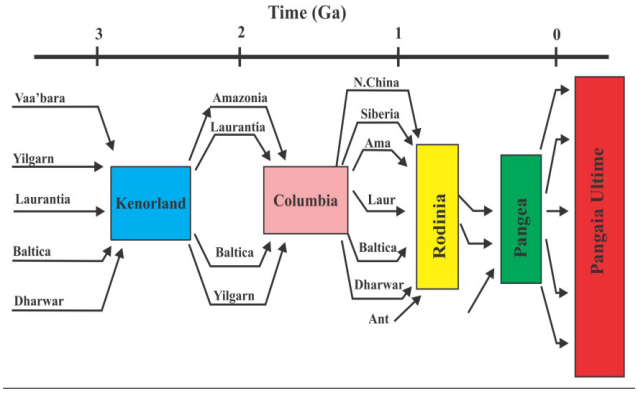

Figure 1.Evolution (assembly-breakup) of the supercontinents through the geological time (From Pesonen et al., 2012)

During the late Mesoproterozoic and Early Neoproterozoic Rodinia Supercontinent assembled through Grenvillian collisional events in span of time ~1100 – 750 Ma (McMenamin & McMenamin, 1990; Hoffman, 1991), with an authenticated final assembly in 1.0 Ga through the continental fragments accretion which later become constituted cratonic components of Gondwana supercontinent (Weil et al., 1998; Zhao et al., 2002b).

The initial time for Rodinia breakup is during 830 – 650 Ma (Hoffman, 1991; Powell et al., 1993; Li et al., 1999; Wingate & Giddings, 2000; Yoshida et al., 2003).

It is well known that precursor magmas of igneous intrusive rocks are sourced from the mantle and document mantle source nature and dynamic information for relationship between crustal and mantle lithospheres (Pearce et al., 1984, Kamber, 2015). Mafic bodies in different sizes occurred in various tectonic regimes and processes response to supercontinents assemblage as small intrusives (subduction, accretion, collision) and a giant intrusives in the breakup of these supercontinents (rifting and breakup) (Ernst et al., 1997, 2008; Ernst and Buchan, 2001; Mayborn and Lesher, 2004; Peng et al., 2007; Zhang et al., 2009; Goldberg, 2010; Hou, 2012; Ernst et al., 2013; Liao et al., 2014). In this work, we investigated two sets of amphibolites from El Obeid area, North Kordofan State, Sudan through detailed study on their geology, petrology, geochemistry, and geochronology to discuss their formation time, mantle sources, petrogenesis and tectonic settings and evaluation and their link with the global Supercontinents reconstruction during the Neoproterozoic.

Geological Background

The structure of the study area comprised Basement Complex, Nawa Formation, Nubian Sandstone, Umm

Rawaba Formation and the superficial deposits (Vail, 1973; Mustafa, 2007). The Basement Complex unit occupies most of El Obeid area and the most intensely deformed part in the south eastern part of the study area in J. Kordofan (Mustafa, 2007, 2018, Figure 2). This unit is the oldest and most extensive sequence with ages ranges between ~2.9 Ga and 1.8 Ga (El Gaby, 1988) generally consists of granites, gneisses, schists, quartzites crystalline limestone and other igneous and metamorphic rocks (Rodis, et al., 1964; Vail, 1973; Abdel Mageed, 1998; Mustafa, 2007). Unconformably a Supracrustal metasedimentary group comprising marbles, amphibolites, schists, and quartzites overland the Basement Complex unit, nevertheless, most of the basement rocks in eastern part of Nuba Mountain are granitic or granodioritic gneisses where metasediments occurred with them, in other portion of this part graphitic schists and siltstones were also recorded (Vail, 1973; Mustafa, 2007, 2018), but no emplacement ages for these rocks had been mentioned in this region. A granitic and syenitic intrusions mass intruded these basements unit northeast of Kalogi in Jebel El Dair, Jebel Dumbeir, Jebel Talodi and limon Hills. The uplift of Precambrian Basement block on the western side of the fault boundary of the Umm Rawaba basin produced the regional E-W dykes of felsite and quartz veins in Jebel Kordofan (Vail, 1973; El Khidir, 1997; Mustafa, 2007, 2018). The weakly foliated grey biotite gneisses, granitic gneisses, pink augend gneisses trending N-S, subdominant N 30° E and Supracrustal sedimentary group with the amphibolites, hornblende schist, graphitic schist, chlorite schist, micaceous quartzites, marbles, siliceous slates and metagabbros are the most distinguished Basement complex unit rocks in Umm Badr-Sodari area. These rocks south of Hamrat Esh Shiekh town intruded by syn- to late-orogenic granites, sheared felsitic extrusives and post-orogenic granites intrusions and volcanic equivalents syenites (El Khidir, 1997). In some parts the low-lying Basement rocks of the Precambrian separated the sedimentary rift basins and sub-basins that encountered in the area and in other parts these basins had been separated by shallow seated basement rocks (Vial, 1978 & 1990). These rocks form an extended dome from the southeast to northwest through the central part of the area separating the two basins in the area from each other (Abadalla, 1999). The Basement rocks in the area were of amphibolite facies which partly retrograde to green schist facies (Rodis et al., 1964; Mustafa, 2007). The low-grade metasediments in Kordofan and the ophiolite in Jebel Rahib were formed with the opening and closing of Red Sea. These rocks were intruded by the Neoproterozoic granitoids between 750 and 550 Ma (Abdel Salam et al., 2002) and `1.0 Ga metamafic dykes (Mustafa, 2018). The study area generally located within the boundaries of Saharan Metacraton and the Arabian Nubian Shield, which are consist of high- to medium-grade gneiss, metasedimentary rocks, migmatite and pockets of granulite (Abdelsalam et al., 2002), that intruded by numerous migmatite and granitic gneiss which metamorphosed on amphibolite facies (Vail, 1971; Schandelmeier et al., 1987; Harms et al., 1990; Abdel-Rahman et al., 1990; Abdelsalam and Dawoud, 1991; Abdelsalam et al., 2002; Küster and Liégeois, 2001; Küster et al., 2008; Ibinoof et al. 2016).

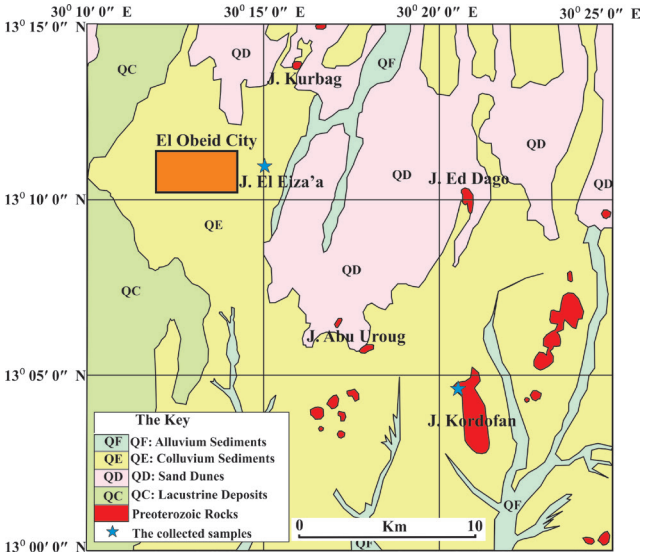

Figure 2.Geological map of the El Obeid area showing the locations of the collected samples and the rock units (modified after Geological Research Authority of Sudan GRAS 2017)

Geology and Petrography of the Amphibolites

The amphibolites in the study area occurred as different lenticular lenses sizes within the Precambrian basements in Kordofan region and can by divided into two groups. Group A is general sheets and bigger in size in J. Eleza'a east of El Obeid near Khor Taggat village and they vary from few meters up to few kilometers (Figures 2, 3a-d), while group B is represented by lenticular lenses within the gneisses and migmatites in J. Kordofan south east of El Obeid (Figure 2). The group of amphibolites which occurred in J. El Eiza'a are displaying anatexis or leucotomies on their outcrops and mostly are dark grey to greenish in colour with banded gneissic structures and medium to coarse-grained textures (Figures 3a,c). Dominantly these group composed hornblende (50-60 %), plagioclase (10-20 %), quartz (~5%) and secondary minerals such as epidote (~2 %) showing fine-grained size aggregates indicating replacement of hornblende (Figure 3d), suggesting medium-grade metamorphism of amphibolite facies. The accessories are represented by apatite and iron oxides.

The group of amphibolites in J. Kordofan occurred as lenticular lenses and don't showed any anataxis or leucotomies on their outcrops, and they are black in colour displaying gneissic structures and medium to coarse-

grained textures (Figures 3e-h). These rocks generally consisted Hornblende (55-65 %), Plagioclase (15-25 %), Quartz (~5%), epidote aggregates and opaque accessories minerals such as iron oxides and apatite (Mustafa, 2018). This group of amphibolites metamorphosed on medium-grade metamorphism of amphibolite facies. Three facies of metamorphism had been distinguished in the study are in response to the metamorphism cycles; medium- to high-grade metamorphism of amphibolite facies during late Archaean/ Neoproterozoic; low-grade metamorphism of green schist facies during the Saharan Metacraton and Arabian-Nubian Shield collision Pan-African and the most recent dynamic activities of green schist facies (El Algeed etal., 1981; Al Beily etal., 1986; El Khidir, 1997; Mustafa, 2007).

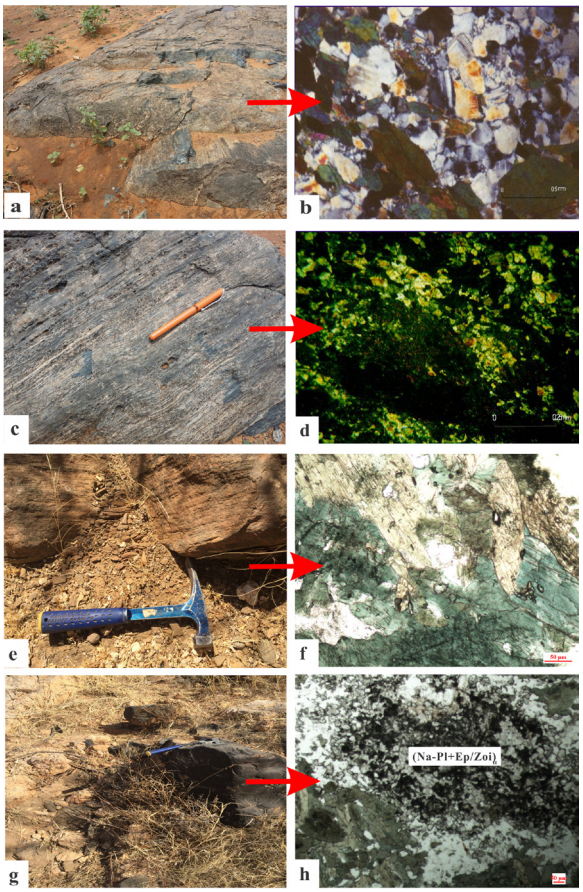

Figure 3.Outcrops and photomicrographs for selected samples from the two amphibolites groups within the gneisses and migmatites in El Obeid area. Group A amphibolites samples showing gneissic structures and anatexis leucotomies with their microstructures showing hornblende alternated to epidote (a-d). Group B amphibolites showing mineral assemblages and alteration of plagioclase (e-h).

Analytical Techniques

Sixteen fresh amphibolite samples were collected from study area in El Obeid area, 8 samples from the outcrops of J. El Eiza'a and 8 samples from J. Kordofan without weak anatexis, avoiding the leucosomes. These samples prepared for the major and trace elements and whole-rock Sr and Nd isotopes analysis. Firstly these samples had been crushed by using a steel mortar, ground an agate mill to < 200 mesh were taken. Major and Trace element abundances for these rock samples were measured at the State Key Laboratory of Geological Processes and Mineral Resources, China University of Geosciences Wuhan by using XRF–1800 and ICP-MS on an Agilent 7500a, respectively. Major elements accuracies of the XRF analyses are estimated to be 1% for SiO_2 and 2%, while analytical methods for trace elements procedures of Liu et al. (2008) had been followed and the ICP-MS analyses for them yield accuracies better than 5%.

Result

Whole Rock Geochemistry

The data of the major and trace element for the both amphibolites groups within the gneisses and migmatites from J. El Eiza'a and J. Kordofan in El Obeid area, North Kordofan, Sudan, are shown in Table 1. The whole rock geochemistry will help us to describe the results that obtained from the geochemical analysis. Moreover, we will highlight the main geochemical features of these amphibolites groups.

Major Elements

Major and trace elements data for these amphibolites groups chemically confirm that they are of igneous origin, suggesting basaltic magmas for their protoliths (Figure 4), and they were weakly alterated.

Group A amphibolites (samples 15HE1, 15HE2, 15HE3, 15HE4, 15HE5, 15HE6, 15HE7 and 15HE8) after normalized to 100% anhydrous, characterized by low MgO = 0.09–0.13, TiO_2 = 0.52–0.92, P_2O_5 = 0.03–0.34 and Mg# (57.0–64.0), with moderate content of SiO_2 = 47.8–49.3wt%, showing TFe2O3= 5.19–8.20 and enrichment in Al_2O_3 =18.6–23.5, Na_2O =1.73–2.39 and depletion in K_2O = 0.11–0.19, with total alkalis and ferromagnesian ranging from 1.90 to 2.55 and 9.89–14.5, respectively. These amphibolites plotted in the traditional igneous classification diagrams which support the meta-igneous nature of the amphibolites total alkalis versus silica (TAS) diagram, they fall within the subalkaline magma series and dominantly in the basalt field, in additional plot on Zr/TiO_2 vs. Nb/Y of the immobile trace elements they also indicated andesitic basalts sub-alkali basalt series (Figures 4a,b), reflecting the mobility of the silicate in some of these amphibolites. The AFM diagram and TiO_2 vs. FeO*/MgO diagram of (Miyashiro, 1975) used for discriminating the Tholeiite and calk-alkaline trends, the majority of these amphibolites group defining Tholeiiteic and calk-alkalinity for some samples as also indicated from the low contents of TiO_2 (Figure 5).

Table 1.Major and trace elements of the two amphibolites groups within the gneisses and migmatites in El Obeid area

Sample	15HE1	15HE2	15HE3	15HE4	15HE5	HE6	HE7	HE8	16HK1	16HK2	16HK3	16HK4	HK5	HK6	HK7	HK8
Major oxides (wt %)																
SiO_2	48.15	47.84	48.74	47.37	47.56	48.54	48.86	47.56	47.2	50.3	50.7	50.5	46.7	47	47	50.6
TiO_2	0.91	0.78	0.77	0.61	0.85	0.51	0.53	0.68	2.43	1.54	1.57	1.62	2.6	2.06	1.98	1.56
Al_2O_3	23.39	22.01	18.4	21.91	21.85	20.72	22.35	22.78	17	14.6	14.4	14.8	15.4	16	13.7	14
TFe_2O_3	5.16	6.29	8.11	6.18	6.99	6.84	5.84	6.49	12.4	13.6	13.8	13.8	13.2	12.4	13.5	14
MgO	4.68	5.36	6.37	5.54	5.25	5.55	4.89	4.35	6.03	7.64	7.6	7.32	5.69	6.83	7.91	6.94
MnO	0.09	0.11	0.13	0.11	0.12	0.12	0.09	0.11	0.19	0.22	0.22	0.22	0.19	0.15	0.18	0.22
CaO	14.8	14.6	13.85	14.75	14.55	13.38	14.33	14.55	13.5	10.4	10.2	10.2	14.4	14.1	14.7	11.2
Na_2O	2.05	2.16	2.33	1.7	2.09	2.36	2.3	2.11	0.67	1.27	1.08	1.06	1.19	0.77	0.57	1.02
K_2O	0.14	0.19	0.19	0.17	0.13	0.13	0.17	0.11	0.25	0.31	0.28	0.29	0.27	0.3	0.24	0.35
P_2O_5	0.08	0.04	0.03	0.04	0.05	0.04	0.03	0.04	0.34	0.12	0.13	0.13	0.31	0.44	0.23	0.13
LOI	0.88	0.47	0.67	0.64	0.46	0.91	1.03	0.48	1.1	0.86	0.8	0.93	0.92	1.5	1.09	0.69
Total	100.33	99.85	99.59	99.02	99.9	99.59	100.42	99.24	101.1	100.9	100.8	100.9	100.9	101.5	101.1	100.7
$Mg^{\#}$	64.2	62.8	60.9	64	59.8	61.6	62.4	57	46.7	50.4	49.8	48.8	43.6	49.8	51.4	47.2
Trace elements (ppm)																
Sc	22.9	24.2	28.3	25.2	21.8	29	20.9	27.3	27.2	63	63.4	60.1	33.4	30.1	29.4	43.7
V	156	179	208	158	206	170	147	183	333	347	355	355	338	251	270	334
Cr	24.9	43.2	62.7	91.3	57.2	81.2	11.8	41.6	186	127	119	118	187	838	499	119
Co	21.4	28.7	32.5	29.7	29	30.5	33.8	25.6	48.2	52.6	53.8	55.5	44.5	68.7	54.6	49.4
Ni	30.2	38.1	45.7	41.7	38	39.2	36.4	32.3	80.5	55.3	53.5	54.7	79.1	500	222	53.7
Rb	4	5	7	4	4	3.85	4.15	4.21	12.1	5.9	5.1	4.9	6.52	20.2	13.4	11.9

Sr	164	137	135	159	134	128	130	134	511	100	100	101	500	347	313	101
Y	22.1	16.6	14.8	14.8	16.4	12.7	11.1	14.1	27	33 .0	35	35	27.8	22.6	20.3	33.1
Zr	34	26	17	21	25	25.6	20.8	24.9	171	87.5	93.8	99	156	135	115	87.9
Nb	0.96	0.7	0.51	0.57	0.63	0.44	0.55	0.46	13	2	2 .00	3	18.7	15.4	15.1	3.01
Ba	26	27	18	30	9	12.5	20.2	8.71	14.7	11.5	9.35	9.98	31.9	10.8	17.1	15.1
La	1.5	1	0.8	0.8	0.9	0.81	0.65	0.91	13	5.94	5.99	6.18	17	14.1	14.2	4.29
Ce	5	3.4	2.7	2.8	3.1	2.61	2.12	3.13	40	7.2	7.4	7.8	39.1	32.3	31.9	12.2
Pr	0.93	0.63	0.5	0.55	0.6	0.49	0.41	0.59	5.4	2	2	2.1	5.07	4.38	4.2	1.88
Nd	5.5	3.8	3.1	3.3	3.7	2.96	2.42	3.48	27.1	11.8	12.5	12.7	23.4	19.3	18.9	10.1
Sm	2.11	1.6	1.29	1.37	1.42	1.21	0.96	1.31	5.55	3.41	3.53	3.61	5.68	4.69	4.77	3.58
Eu	1.1	0.76	0.61	0.65	0.72	0.5	0.56	0.76	1.77	1.16	1.23	1.21	1.88	1.6	1.49	1.19
Gd	3.12	2.29	1.98	1.97	2.2	1.59	1.34	1.82	5.44	3.98	4.18	4.2	5.48	4.71	4.42	4.57
Tb	0.57	0.42	0.35	0.37	0.41	0.33	0.27	0.35	0.92	0.83	0.87	0.87	0.89	0.76	0.72	0.85
Dy	3.86	2.99	2.59	2.54	2.91	2.11	1.81	2.43	5.32	5.61	5.89	5.96	5.3	4.37	4.11	5.67
Ho	0.82	0.62	0.56	0.54	0.6	0.48	0.4	0.5	1.01	1.21	1.26	1.27	1.03	0.84	0.75	1.22
Er	2.3	1.82	1.61	1.56	1.8	1.22	1.1	1.39	2.79	3.47	3.7	3.74	2.71	2.19	1.95	3.4
Tm	0.36	0.27	0.24	0.23	0.26	0.21	0.18	0.22	0.42	0.58	0.61	0.61	0.38	0.32	0.28	0.52
Yb	2.34	1.67	1.53	1.51	1.75	1.34	1.15	1.43	2.44	3.5	3.69	3.67	2.42	1.91	1.65	3.44
Lu	0.34	0.26	0.23	0.23	0.25	0.19	0.17	0.22	0.36	0.53	0.56	0.56	0.36	0.27	0.23	0.49
Hf	1.14	0.88	0.62	0.74	0.88	0.75	0.7	0.81	4.22	2.44	2.58	2.71	3.93	3.45	3.04	2.58
Ta	0.08	0.05	0.04	0.04	0.05	0.05	0.04	0.05	1.42	0.26	0.28	0.28	1.15	0.92	0.94	0.23
Pb	1.9	0.8	1.4	1.5	0.6	0.5	1.04	0.65	6.05	3.48	3.97	4	5.94	6.32	2.98	3.21

Th	0.1	0	0	0.2	0	0.05	0.05	0.04	1.62	0.53	0.53	0.57	1.5	1.23	1.22	0.53
U	0.04	0.03	0.01	0.02	0.02	0.03	0.03	0.03	1.27	0.14	0.15	0.16	0.84	0.97	0.58	0.15
Ratios																
Ba/Nb	27.3	38.9	35.9	51.9	13.7	28.4	36.8	18.8	1.1	5.02	3.77	3.82	1.71	0.7	1.14	5.02
La/Nb	1.61	1.4	1.63	1.46	1.4	1.84	1.19	1.96	0.97	2.59	2.42	2.37	0.91	0.92	0.94	1.43
Th/Nb	0.08	0.07	0.06	0.32	0.05	0.11	0.08	0.09	0.12	0.23	0.21	0.22	0.08	0.08	0.08	0.18
Th/Ta	1.01	0.89	0.8	4.35	0.67	1.05	1.08	0.86	1.14	2.04	1.89	2.04	1.3	1.33	1.3	2.31
La/Ta	20.3	19	21.2	19.9	17.5	17.1	15.6	18	9.2	22.8	21.4	22.1	14.8	15.3	15.1	18.8
La/Yb	0.66	0.59	0.54	0.55	0.51	0.61	0.56	0.63	5.33	1.7	1.62	1.68	7.03	7.4	8.61	1.25
Zr/Nb	35.2	36.9	33.1	36.8	40	58.3	38.1	53.9	12.8	38.2	37.8	37.9	8.4	8.8	7.6	29.3
Zr/Sm	16.1	16.2	13.1	15.3	17.9	21.1	21.7	18.9	5.55	3.41	3.53	3.61	5.68	4.69	4.77	3.58
Zr/Hf	29.6	29.4	27.1	28.5	28.7	34.1	30	30.9	40.5	35.9	36.4	36.5	39.8	39.2	37.8	34.1
Lu/Hf	0.3	0.29	0.36	0.32	0.29	0.25	0.25	0.27	0.09	0.22	0.22	0.21	0.09	0.08	0.08	0.19
Ba/Zr	0.78	1.05	1.09	1.41	0.34	0.49	0.97	0.35	0.09	0.13	0.1	0.1	0.2	0.08	0.15	0.17
Eu/Eu*	1.31	1.22	1.16	1.21	1.25	1.09	1.51	1.5	0.97	0.96	0.97	0.94	1.01	1.03	0.97	0.89
Ti/V	148	100	74.7	96.3	84.5	74.2	73.9	79.5	18.2	20.9	21.3	21.4	18.3	20.2	16.7	21.9
(Hf/Sm)n	0.78	0.79	0.7	0.77	0.9	0.89	1.04	0.88	1.09	1.03	1.05	1.08	1	1.06	0.92	1.03
(Ta/La)n	0.82	0.88	0.79	0.84	0.96	0.98	1.08	0.93	1.83	0.73	0.78	0.76	1.14	1.09	1.11	0.89
(La/Th)n	2.5	2.64	3.26	0.57	3.21	2.01	1.78	2.59	0.99	1.39	1.4	1.34	1.41	1.43	1.44	1.01
(La/Ce)n	0.79	0.76	0.78	0.76	0.74	0.8	0.79	0.75	0.84	2.15	2.1	2.06	1.12	1.13	1.15	0.91
(La/Yb)n	0.47	0.42	0.39	0.4	0.36	0.43	0.4	0.45	3.82	1.22	1.16	1.21	5.05	5.31	6.18	0.9

TFeO = 0.8998TFe2O3, Mg# = [100(MgO/40.3)]/[MgO/40.3+FeO/71.8], Eu/Eu* = (Eu)cn/[(Gd)cn +(Sm)cn/2, cn-chondrite normalized; n-primitive mantle normalized

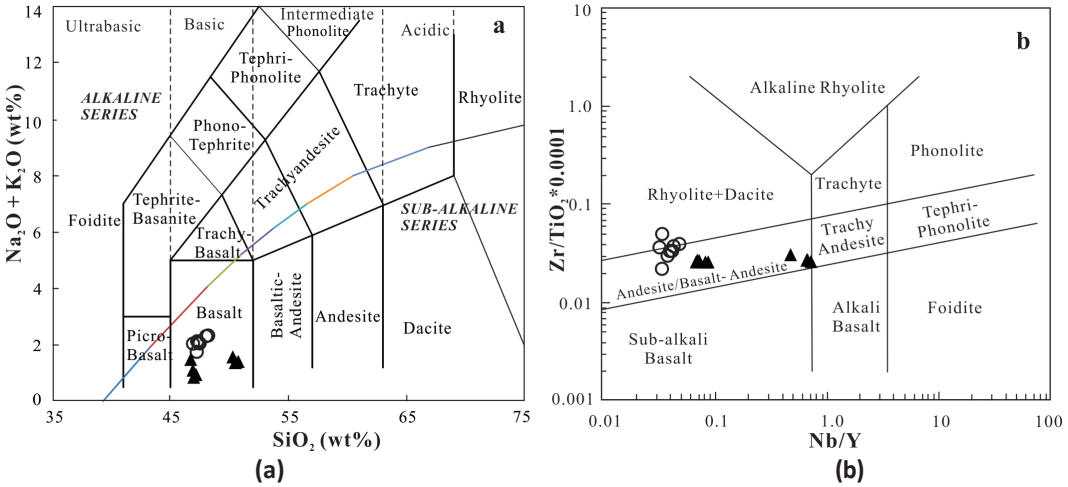

Figure 4.Plots on (a) TAS and (b) Zr/TiO2 vs. Nb/Y of Pearce (1996) for the two amphibolites groups within the gneisses and migmatites in El Obeid area

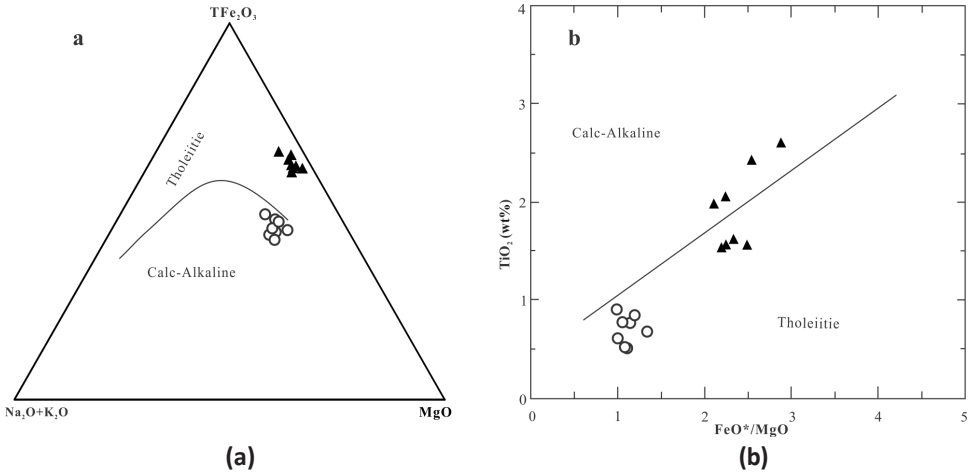

Figure 5.(a) AFM diagram of Irvine and Baragar (1971). (b) TiO2 vs. Fe*/Mg of (Miyashiro et al., 1975) for the two amphibolites groups within the gneisses and migmatites in El Obeid area.

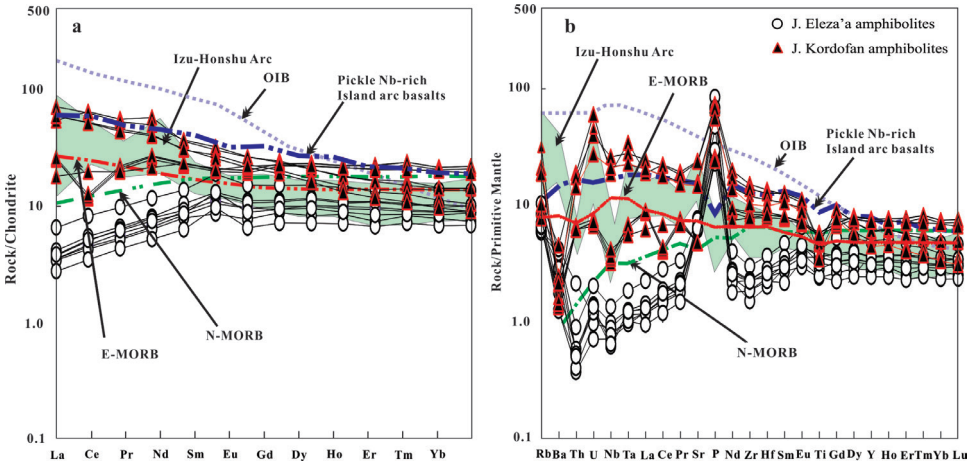

Figure 6.(a) Chondrite-normalized REE diagram and (b) primitive mantle-normalized incompatible-element Spider diagram for the two amphibolites groups within the gneisses and migmatites in El Obeid area. The normalization values of chondrite and primitive mantle and the data for Ocean Island Basalt (OIB), Normal Mid-Ocean Ridge Basalt (N-MORB) and Enriched Mid-Ocean Ridge Basalt (E-MORB) are from Sun and McDonough (1989). Data for the, Izu-Honshu Arc Pickle Nb-rich island basalts are from Gust (1997) and Hollings and Kerrich (2004)

This group displayed low Ni and Cr contents (30.2–45.7 and 11.8–91.29ppm) and Zr/Hf & Ti/V ratios (27.1–34.1 and 73.9–148), respectively. The REE patterns for this group amphibolites displaying positive Eu anomaly (Eu/Eu*=1.09–1.50), and show LREE enrichment $(La/Yb)_n$ = (0.36–0.47) (Figure 6a) with ΣREE contents from (13.6 to 30.0). On the primitive mantle normalized spider diagram, these rocks show large-ion lithophile elements (LILE) enrichment, negative (Th and Ti) anomalies, positive (Pb and P) anomalies and high contents of Rb and Ba, with slightly Nb-Ta and Zr-Hf troughs, relatively indicated their similarities with Arc-volcanics (Figure 6b).

The group B amphibolites (samples 16HK1, 16HK2, 16HK3, 16HK4, 16HK5, 16HK6, 16HK7 and 16HK8) almost have the same major and trace elements contents, but they have the higher contents of TFe2O3 = 12.4–14.0 wt% and Na_2O = 1.30–2.71 wt%, P_2O_5 = 0.13–0.44 wt%, and TiO_2 = 1.54–2.06 wt%, the lower contents of Al_2O_3 = 12.77–16.17 wt %, MgO = 4.07–6.35 wt% and CaO = 7.68 – 9.51 wt%. The contents of SiO_2 are 48.2 – 54.7 wt%, K_2O = 0.73 – 1.61 wt%, with total alkalis and ferromagnesian ranging from 2.14 to 4.23 wt% and 18.92 –26.61 wt%, and $Mg^{\#}$ = 29.98 – 51.58. These amphibolites in (TAS) diagram (Figure 4a), show subalkaline magma series plotted within basalt and basaltic andesite fields, while on Zr/TiO_2 vs. Nb/Y diagram they show sub-alkali basalt affinity (Figure 4b). On Miyashiro (1975) diagrams (Figure 5b), these amphibolites were plotted along the tholeiitic trajectory confirming that these subalkaline basalts were tholeiitic. The low Mg# values from 29.98 to 51.58, Ni and Cr = 17.7–87.2 and 11.2–183 ppm, respectively and low contents of MgO ≤ 7.26 wt% for these amphibolites, respectively, indicating evolved protolith magma (Ahijado et al., 2001).

The garnet-bearing amphibolite characterized by Zr/Hf and Ti/V ratios of 36.7 – 40.3 and 27.5 – 38.7, respectively, and also displayed negative Eu anomaly (Eu/Eu*= 0.61 – 0.92), showing LREE enrichment $(La/Yb)_n$ = 2.75 – 9.34 (Figure 6a) with ΣREE contents from 121.1 to 203.5. They also displayed large-ion lithophile elements (LILE) enrichment on the primitive mantle normalized spider diagram, with negative P, Ti, Nb-Ta and Zr-Hf anomalies, positive Th anomaly and high contents of Rb and Ba, relatively indicated their similarities with Stromboli basalts (Francalanci et al., 1999), the Arc-volcanics and Pickle Nb-enriched basalt (Figure 6b).

Discussion

Petrogenesis

The both amphibolites groups display moderate Tb-Yb (Table 1) $Tb/Yb_{(cn)}$ ratios are >1 higher of the chondritic (1.05 – 1.98, and 0.23 for the chondrites, Boynton, 1984). This suggests that no one of olivine, orthopyroxene, clinopyroxene and plagioclase were major fractionating minerals in the petrogenesis of both groups of these amphibolites but only amphibole and garnet were probably the major crystallising assemblages.

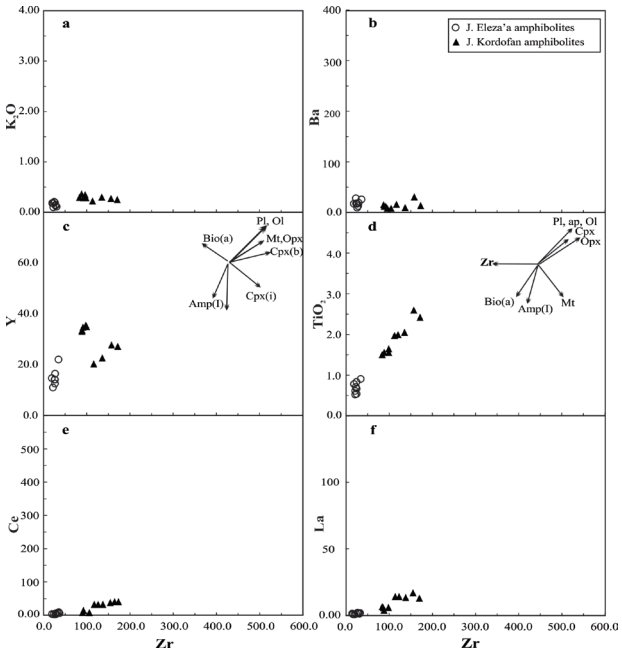

Figure 7.Plots of selected minor and trace elements vs. Zr (differentiation indices) for the two amphibolites groups within the gneisses and migmatites in El Obeid area. Fractionation vectors are after Pearce and Norry (1979). pl plagioclase, ol olivine, mt magnetite, opx orthopyroxene, cpx clinopyroxene, ap apatite, amp amphibole, bio biotite, zr zircon; b, i and a represent fractionation trends in basic, intermediate and acid magmas respectively

As mentioned before the group A amphibolites were Cal-alkaline to Tholeiitic, while group B indicated both trends in the AFM and plot of Irvine and Baragar (1971), with slightly different magmatic fractionation magma series trends (Figure 5). Group B amphibolites clearly are richer in Y, Ce, La, Sr, Ti and Mn but tend to be poorer in Na and Ca, compared with the group A amphibolites (Table 1; Figure 7). Further, Group B amphibolite is much richer in REE (ΣREE = 51.1 to 11.5 and 13.6–30.0 for group A), and has a small negative Eu anomaly (Eu/Eu* = 0.89–1.03), beside group A which displays an insignificant positive Eu anomaly (Eu/Eu* = 1.09–1.50). The enrichment and poor contents of the above mentioned elements indicates the relationship of the fractionation in both two groups of amphibolites, but they cannot be more evolved crystallizations from the same basaltic magma where they formed, because they also have variable contents of Co, Ni and Cr signifying differentiated end-members. Also the petrological evidence of these two groups' reasonably explanted differences is which they were evolved separate magma series. Plots on Zr as a stable fractionation index against K_2O, Ba, Y, TiO_2, Ce and

La (Figure 7) both groups were more scattered and unclear characterizing by K_2O < 1 wt% and average of minerals fractionation trends in combine with their REE patterns obviously indicating an igneous origin for the two groups.

Nature and Origin of the Amphibolites

The both two groups of the amphibolites from J. El Eiza'a and J. Kordofan showed scattered and ambiguous origin sources, data of the major and trace element Table 1. These amphibolites displayed LOI contents <2.00 wt% and a narrow range of alteration, indicating weak rule of the fluid-related alteration on these rocks.

In general the discrepancy between ortho- and para-amphibolite is possible by the relict igneous or sedimentary features remaining. These features can by physical or geochemical, physically such as discordant contacts, sedimentary bedding or relict phenocrysts, and chemically in nature of the elements stability. The relict features in high grade metamorphism are difficult to diagnose (Walker et al,. 1960; Orville, 1969; Foster, 1994), and only immobile elements inherited from igneous or sedimentary precursors will survive these conditions of metamorphism. Petrographically the of amphibolites origin (Turner and Verhoogen, 1960), the presence of relict phenocrysts shows an igneous origin, while the presence of banding is commonly is assign of a sedimentary origin, although these evidences were not enough. Mineralogically, sedimentary origin would be indicated by a high ratio of hornblende to plagioclase, abundant pyroxene and calcium rich accessory minerals such as garnet, epidote, scapolite or calcite. Titanium-rich phases such as sphene or illmenite would suggest an igneous origin. The mineralogy is not enough to establish a protolith for the studied amphibolites have a high proportion of hornblende to plagioclase, which would tend to indicate a sedimentary origin. On the other hand, mostly these amphibolites contain accessory minerals such as sphene and metallic opaques, which are generally attributed to igneous derivation. All our petrography and geochemistry investigations have discriminated the Delingha amphibolites are derived from sub-alkaline basalts, as an igneous origin.

Moreover, the studied amphibolite situated within the amphibolite-facies rocks that underwent polymetamorphism cycles with some metasomatism processes and retrogressive of plagioclase which made changes on them. Most of the chemical elements such as the Large-Ion-Lithophile Elements (K, Na, Ca, Rb, Ba and Sr) effected by the metamorphic factors during the metamorphism processes, while averagely change made on the transition metals (Cr, Ni, Co and Sc), the Rare Earth Elements, and the High Field Strength Elements (Ti, P, Zr, Y, Nb and Ta) and generally they will still stable during these conditions (Cullers et al., 1974; Floyd and Winchester, 1978, 1983; Weaver and Tarney, 1981; Thompson, 1991; Rollinson, 1993 Staudigel et al., 1995; Ahmed-Said and Leake, 1997; Kelley et al., 2003). Otherwise, their initial suite and fractionation trends will redistributed in case of any addition or removal of these or other incompatible elements (Wood et al., 1981) , so the investigation of these elements will use the mobile and the immobile elements.

The low SiO_2 and K_2O contents and high abundances of Fe_2O_3, MgO and CaO for both amphibolites groups suggested a basaltic nature for their precursor magmas. Moreover, they are classified as sub alkaline basalts on the TAS (Figure 4a), plots on Zr/TiO_2 *vs*. Nb/Y diagram of Winchester & Floyd (1977) that revised by Pearce (1996) show that both sets are andesite to andesitic basalts (Figure 4). These sub alkaline basalts in the AFM and plot of Irvine and Baragar (1971) group A amphibolites are dominantly calc-akaline and indicated a broad Tholeiite trend on TiO_2 *vs*. FeO*/MgO diagram (Figure 5), in contrary, group B amphibolites showed Tholeiite affinities in the AFM plot and Cal-alkaline to Tholeiitic affinities on TiO_2 *vs*. FeO*/MgO diagram due to their low TiO_2contents (Figure 5).

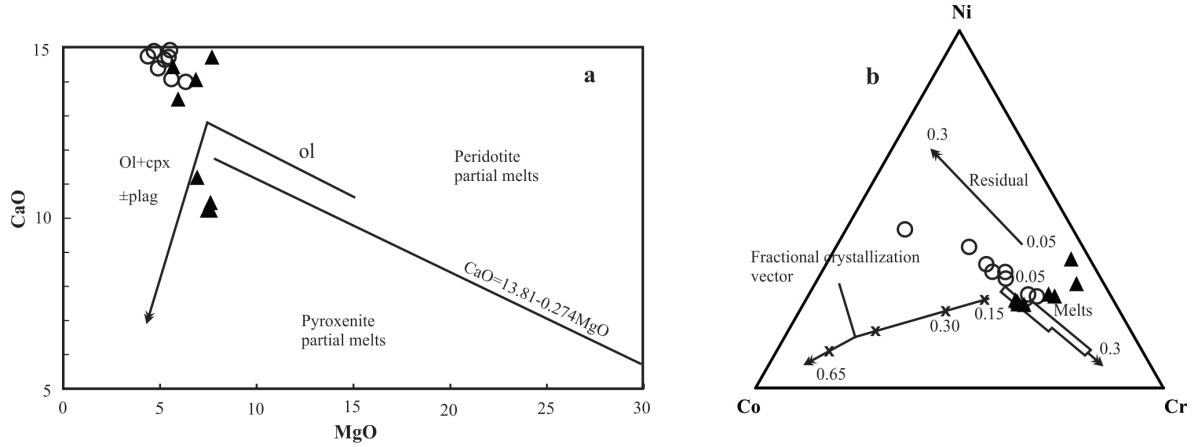

Figure 8.Plot on (a) CaO vs. MgO diagram of Herzberg and Asimow (2008) (b) the Ni-Co-Cr diagram of Jagout et al. (1979) for the two amphibolites groups within the gneisses and migmatites in El Obeid area

Fractional Differentiation

Primary magmas characterized by high Mg# (68–72) and high Ni (300–600 ppm) and Cr (~1000 ppm) contents (Frey et al., 1978; Gill, 2010). Metamorphic rocks that derived from mafic magmas with low MgO, Mg#, Ni and Cr, probably suggested fractional differentiation of some minerals in their magma before its ascending through and intrusion into the continental crust, indicating evolved magmas rather than primary magma (Ahijado et al., 2001). Both two amphibolites groups contain low values of those of the primary magmas, they characterized by Mg# (57.0–64.2 and 43.6–51.4), Ni (30.2 –45.7 and 53.5–500 ppm) and Cr (11.8–91.29 and 118–838 ppm) for group A and B, respectively. The fractional crystallization is noticeable in related variation diagram of Cao with MgO and the three indicator minerals in the primitive mantle (Figure 8a), also the moderate negative to no Eu anomalies in Chondrite-normalized REE pattern for these amphibolites groups (Figure 6a) might indicate partial melting process.

Moreover, both amphibolite groups relatively characterized by geochemical signatures that represent the magma involvement of recycled crust in the mantle source for their protoliths, e.g., TiO_2 concentrations (0.52–0.92 and 1.54 – 2.60%), high Nb/Ta (9.18–13.5 and 8.81–16.7), enrichment in Nb and Ta indicated by Nb/La (0.51–0.84 and 0.39–1.10) for group A and slightly higher for group B, respectively. These geochemical features and the physical nature of their source had been evaluated by the CaO vs. MgO diagram of Herzberg and Asimow (2008) which suggested fractional differentiation (Figure 8a). The two amphibolites groups according to their MgO contents which are <10% show chemical composition consistent with fractional crystallization of clinopyroxene +olivine ± (plagioclase), considered incompatible documentation of their source lithology, suggesting involvement of a basic source. Generally partial melts might cases decreasing of CaO concentrations, which explained the Ca-clinopyroxene and olivine fractionation. The enriched component of the both amphibolites protoliths had been derived from the recycled crust introduced by primitive mantle that experienced fractional crystallization (e.g. Herzberg, 2006; Gurenko et al., 2009) this deduced according to distribution of recycled basic rocks in the mantle, which slightly similar to the protoliths of the studied amphibolites in El Obeid area. Furthermore, group A amphibolites relatively plotted on the residual side of the diagram and have the primitive mantle of Jagout et al. (1979) trend also some samples of this group representing primary melts while group B amphibolites indicated melt processes (Figure 8b). The distributions of these two groups suggest that these amphibolites formed from different fractionation processes.

Heterogeneous Mantle Sources

The both two groups of amphibolites were derived from different mantle sources because completely they have different REE and spider diagram patterns. Group A amphibolites on chondrite-normalized are characterized by similar REE patterns (Figure 6a), suggesting parental magmas. ΣREE contents of these amphibolites vary obviously between 13.6 and 30.0 ppm, with slight depletion of LREE relative to HREE ((La/Yb)n = 0.36–0.47) and positive Eu anomalies (Eu/Eu* = 1.09–1.50), similar to a typical N-MORB (Sun & McDonough 1989). However, on primitive mantle-normalized multi-element patterns, this group showed slightly enrichment of LILE (Rb, Ba, U), with strongly positive Pb, Ti, P and moderate Nb–Ta and Zr–Hf anomalies and display remarkable spiky patterns of a typical N-MORBs. Group B amphibolites are characterized by irregular enriched chondrite-normalized REE patterns (Figure 6a), their ΣREE contents ranges from 51.1 to 11.5 ppm, with slight depletion of LREE relative to HREE ($(La/Yb)_n$ = 0.90–6.18) and negative to positive Eu anomalies (Eu/Eu* = 0.89–1.03). This group on the primitive mantle normalized incompatible-element spider diagram, characterized by slightly enrichment of LILE (Rb, Ba, U), with strongly positive P, negative Ti, and an obvious Nb–Ta and Zr–Hf anomalies displaying significant spiky patterns similar of E-MORBs (Figure 6b). Both groups of amphibolites were generated on arc tectonic settings related to subduction processes (Mustafa et al, 2018, 2019) for discriminating source variation, effects of partial melting, recognition of subduction-related components and the influence of crustal contamination for these groups pots on Th/Yb vs. Nb/Yb, Nb/Y vs. Zr/Y and the Zr/Nb vs. La/Yb. Group A indicated within-plate enrichment on Th/Yb vs. Nb/Yb and when plotted in the Th/Yb vs. Nb/Yb diagram of Pearce and Peate (1995) indicated an enriched mantle falling inside the mantle array (Figure 9a), they extent slightly along the within-plate enrichment. The heavy diagonal lines of constant display the array of basalts were from non-subduction settings which derived either from either enriched (i.e., OIB) or depleted mantle (i.e., MORB) sources. Also the low Nb/Y and Zr/Y ratios are other criteria for presence of enriched components in the source (Wilson, 1993). Plots on the Nb/Y vs. Zr/Y and La/Yb vs. Zr/Nb diagrams indicated that the source of the protoliths of group A amphibolites was slightly heterogeneous from N-MORN, E-MORN, Primitive mantle and OIB affinities (Figures 9b, c), the heterogeneity is also represented by the wide separate of the incompatible elements ratios for these amphibolites. Plot on Th/Yb vs. Nb/Yb diagram after Yang et al. (2014) is also suggested enriched mantle source for these rocks in active continental margin alkali oceanic areas (Figure 9d).

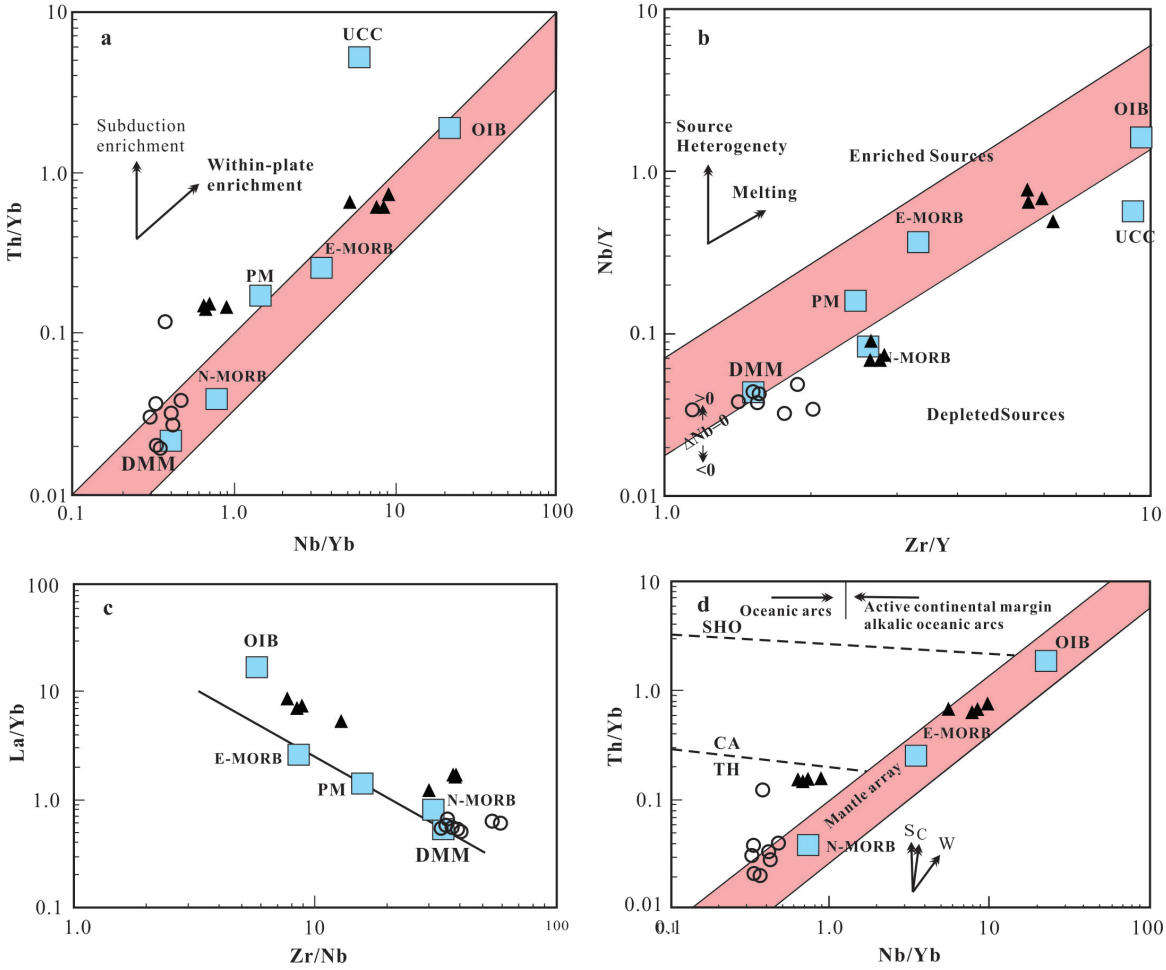

Figure 9.Plots of the two amphibolites groups within the gneisses and migmatites in El Obeid area on: (a) Th/Yb vs. Nb/Yb diagram of Pearce and Peate (1995) the heavy diagonal lines of constant Th/Nb show the array of basalts from non-subduction settings (shaded) derived from either enriched (i.e., OIB) or depleted mantle (i.e., MORB) sources, while vectors indicate the influence of subduction component and within-plate enrichment. (b) Nb/Y vs. Zr/Y diagram after Fitton (2007), the parallel lines mark the limits of the Iceland array and the DNb = 0 line separating enriched (E- MORB, OIB) from depleted (N-MORB) sources, while vectors are from Escuder Viruete et al. (2009). (c) La/Yb vs. Zr/Nb diagram the heavy solid line shows the array for mantle- derived basalts generated from depleted (DMM) or enriched (PM) sources. (d) Th/Yb vs. Nb/Yb diagram after Yang and santosh (2014)

Group B showed enrichment to depleted mantle (Figure 9a), they extent slightly along the subduction enrichment. This group is slightly a homogeneous source derived from depleted mantle (Figure 9b,c); this homogeneity is also indicated by their incompatible elements ratios limitation. These amphibolites also showed enriched mantle source in oceanic area (Figure 9d).

Both groups of these amphibolites indicated partial melting processes from the increasing of their incompatible elements proportions to less-incompatible elements (e.g., Pearce and Norry, 1979; Aldanmaz et al., 2006), the high Zr/Y and low Zr/Nb partial melting for these groups (Figure 9 b) point to and show strong amounts of melt (Ilnicki, 2010; 2011) were made in their source. Their Zr/Nb and Zr/Y ratios are also suggest little variation in the degree of partial melting. In the La/Yb vs. Zr/Nb diagram these amphibolites plotted them above the mantle array (Figure 9c), indicating that the melting processes generated in the mantle garnet facies (Aldanmaz et al. 2006). In addition, the heterogenetic source of these two groups had been recognized when they plotted on Ti_2O vs. CaO/Ti_2O and Al_2O_3/Ti_2O of Sun and Nesbit (1978), group A correspond tectonically with areas defined by arc from depleted sources, while group B were correspond with an undepleted source (Figures 10a,b). In summary, we can prove that the precursor basalts of the two amphibolites groups from El Obeid area were originally derived from different mantle sources of extremely depleted young mantle, relatively old but moderately depleted lithospheric mantle and old enriched mantle that have been metasomatized by subduction-related melts.

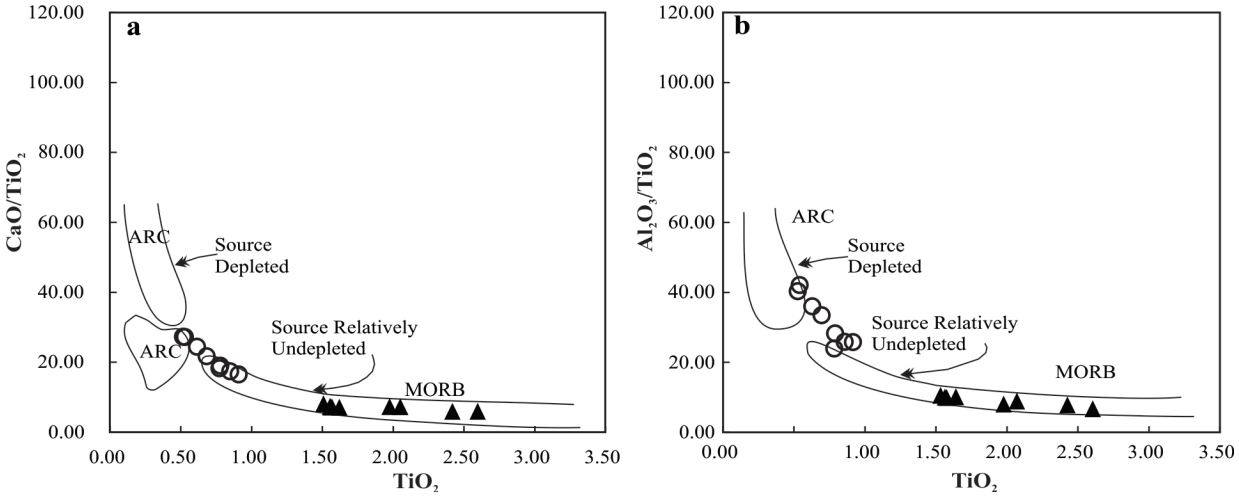

Figure 10.Plot on (a) on Ti2O vs. CaO/Ti2O and (b) Al2O3/Ti2O of Sun and Nesbit (1978) for the two amphibolites groups within the gneisses and migmatites in El Obeid area

Tectonic Settings

The both amphibolite groups in El Obeid area located within the Precambrian rocks indicating that their precursor magmas should be derived from an old lithospheric mantle. Their precursor magmas protoliths were emplaced during Neoproterozoic period at ~1.00 Ga, which is consistent with the age of ~0.997 Ma of the youngest detrital zircon from group A amphibolites (Mustafa et al., 2018, 2019). Both groups indicated tholeiitic to calc-akaline trends of basalts (Figures 4a,b) as assign of the basaltic volcanism of primitive to more mature oceanic convergent margin of oceanic island arc and/or back-arc setting (Küster and Liegeois, 2001). Their primitive mantle-normalized incompatible element patterns (Figure 6b) indicated typical arc settings (Mcculloch and Gamble, 1991; Francalanci et al., 1999) approximately related to a subduction tectonic setting.

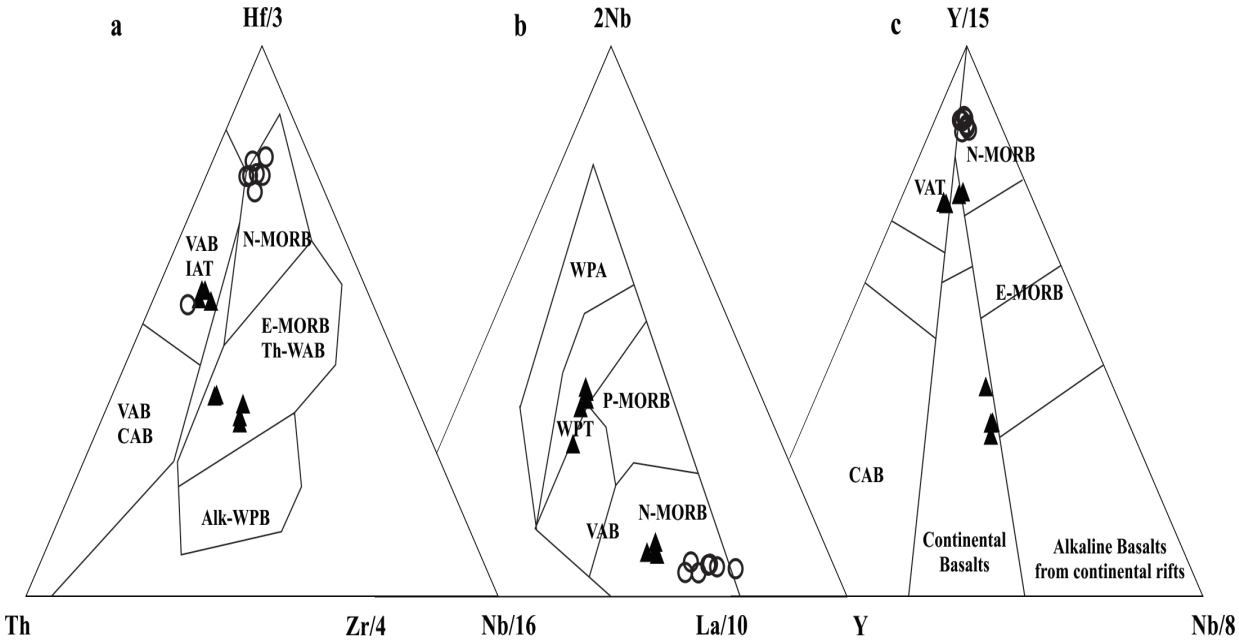

Figure 11.Tectonic discrimination diagrams (a) Hf–Th-Nb of Wood (1980). (b) Nb-Zr-Y of Meschede (1986). (c) Y-La-Nb of Cabanis and Lecolle (1989) for the two amphibolites groups within the gneisses and migmatites in El Obeid area. Alk-WPB alkaline within-plate basalts, CAB calc-alkaline basalts, CFB continental flood basalts, CRB continental rift basalts, E-MORB enriched MORB, IAB island arc basalts, IAT island arc tholeiites, N-MORB normal MORB, OIB ocean island basalts, P-MORB plume MORB, VAT volcanic arc tholeiites, VAB volcanic arc basalts, WPB within-plate basalts, WPT within-plate tholeiites, Th-WPB tholeiitic within-plate basalts

The occurrence of these amphibolites sporadically associated with metasediments rocks as analogues and small scale size (Figures 3a,c,e,g), suggesting that they were likely related to volcanic edifices in subduction settings or back-arc environments (Ernst et al., 1995; Peng et al., 2007) rather than to products of breakup of any supercontinents. The primitive mantle-normalized multi-element patterns (Figure 6) for these amphibolites tend to arc basalts or island arc tholeiites (Gust et al., 1997; Hollings and Kerrich, 2004). Moreover, these amphibolites discriminated as calk-alkaline to tholeiite sub-alkaline rocks (4). In addition, plot on Hf-Th-Nb diagram of Wood. (1980) group A amphibolite were plotted in the VAB, IAT and E-MORB fields, and N-MORB for vast samples of group B amphibolites with IAT affinities (Figure 11a). However, plots on Nb-Zr-Y diagram of Meschede. (1986) showed within plate tholeiite, P-MORB and N-MORB, group B indicated N-MORB (Figure 11b), plot on Y-La-Nb diagram of Cabanis and Lecolle. (1989) also indicated N-MORB group B amphibolites, while VAT and Continental Basalts are the discriminations of group A amphibolites (Figure 11c). Therefore, geological occurrence and scale, ratios of some typical elements and comprehensive discrimination results all point to volcanic arc setting for generation of the precursor magmas of the protoliths of the two amphibolites groups in El Obeid area.

Significance of these Amphibolites with Rodinia Evolution

The basement Complex of the study area which located in North Kordofan, Sudan, metamorphosed in amphibolite facies with locally anatexis during the Neoproterozoic time, coevally with Rodinia supercontinent reconstruction. These amphibolites occurred within the boundary suture of the collision and subduction between the Saharan Metacraton and ANS the Arabian-Nubian Shield (Schandelmeier et al., 1990, 1994; Abdel-Rahman et al., 1990b; Stern, 1994). ANS comprised two lithologic units; Island-arc/back-arc basin and Ophiolite assemblages (Abdelsalam et al., 2002). The collision and subduction between these two blocks resulted deformation (Vail, 1971, 1972; Schandelmeier et al., 1987, 1988; Stern, 1994; Abdelsalam and Stern, 1996a, b; Abdelsalam et al., 1998; 2002), metamorphism (Kröner et al., 1987a,b; Stern and Dawoud, 1991) and magmatism (Stern, 1994) reworking the Neoproterozoic rocks. Furthermore, this continental crust was affected by extension to form restricted oceanic basins, which subsequently closed by the collision between drifted blocks. The study area is also affected by this reworking (El Khidir, 1996; Abdelsalam et al., 2002; Mustafa, 2007; Eivok, 2013; Ibnoof et al., 2016), nevertheless, during formation of the Arabian-Nubian Shield, the reworking of East Saharan Craton in North Africa and the formation of Mozambique Belt in Central and South Africa East African there are Orogen origination event. This orogeny started with the breakup of Rodinia Supercontinent ~900-850 Ma to share in forming Gondwana supercontinent. In response to this collision the juvenile crustal in that period ophiolites in ANS were formed due to the arc accretion and amalgamation (Stern, 1994; El Khidir, 1997; Mustafa, 2007, 2018). The opening and closing of Red Sea has a big rule in the formation of the ophiolite in Jebel Rahib and low-grade sedimentary belt in Kordofan in central Sudan, later these rock sequences were intruded by the Neoproterozoic granitoids between 750 and 550 Ma (Abdel Salam et al. 2002).

The remobilization of the Saharan Metacraton understood through four models; collision; Delamination of the sub-continental mantle lithosphere; extension; and assembling of the metacraton from exotic terranes with further post-collisional dismembering (Abdelsalam et al. 2002). Bayuda region represented the eastern extension of Saharan Metacraton collision side with the ANS along Keraf Zone in Sudan (Abdelsalam and Stern, 1996b; Evuk, 2013). The island-arc/back-arc marginal settings and low-grade volcano-sedimentary rocks within the medium to high-grade gneissic terranes which is similar to those of ANS also represented the accretion processes on the eastern margin of the Saharan Metacraton (Küster and Liégeois, 2001). The boundary between the Saharan Metacraton and ANS in Sudan also observed along Zalingei Fold Zone or further west (Küster and Liégeois, 2001), which is occasionally involved Kordofan region where these amphibolites cropped out. The sequence evolution of the Red Sea Hills sector of ANS divided into three periods; Early (1200-1000 Ma); Middle (1000-600 Ma) and Late Pan African (600-500 Ma) (Abdel-Rahman, 1993), parallel to the events that supporting ophiolite-arc collision accretion model (Gass, 1981; Abdel-Rahman, 1993; Evuk, 2013). The suture zones in the north and northeast Sudan are resulted from the island-arc/back-arc basin complexes and plate margin type volcano-sedimentary rocks which are in a tectonic contact with the ophiolitic rocks as well as vast sutures in north and northeast Sudan occur in the region (Kroner, 1985; Ries et al., 1985; Stern et al., 1989, 1994; Harms et al., 1994; Schandelmeier et al., 1994; Evuk, 2013). The North Kordofan region is not famous by such kind of sutures, but the formation of these amphibolites is similar to overall processes in the Sudan region.

Group A amphibolites within the basement of Kordofan region were formed at ~997 Ma (Mustafa et al., 2019) which coevally with Rodinia supercontinent assemblage. Moreover, both groups of these amphibolites characterized by moderate- to high-iron content, with distinctive spiky and arc-like primitive mantle-normalized incompatible-element patterns, and are calc-alkaline to tholeiitic basalts equivalent with those of the Bayuda Desert amphibolites signifying basaltic volcanism of primitive to more mature

oceanic convergent margin of oceanic island arc and/or back-arc setting (Küster and Liegeois, 2001). These amphibolites were derived from a complex mantle source with components having a mildly depleted mantle nature indicating that their precursor magma of island arc to back arc environment. Therefore, we consider that the emplacement of these rocks during the Neoproterozoic time with the Rodinia supercontinent evolution exactly at ~997 Ma (Mustafa et al., 2019) encountered associated with the Bayudian event (Rahaba-Absol Terrane) during the Rodinia assemblage, which represent a time of mixed magmatism and metamorphism.

Conclusion

The amphibolite within the Basement Complex of El Obeid area in North Kordofan, Sudan petrologically and geochemically had been divided into two groups. Group A amphibolites has typical N-MORBs, while group B characterized E-MORBs patterns Both groups of amphibolites were generated on arc tectonic settings related to subduction processes. Group B showed enrichment to depleted mantle, group A correspond tectonically with areas defined by arc from depleted sources, while group B were correspond with an undepleted source. In summary, we can prove that the precursor basalts of the two amphibolites groups from El Obeid area were originally derived from different mantle sources of extremely depleted young mantle, relatively old but moderately depleted lithospheric mantle and old enriched mantle that have been metasomatized by subduction-related melts. These amphibolites were sub-alkali to Tholeiite basaltic magmas that derived from subduction-induced melt-related enrichment sub-continental lithospheric mantle that indicated arc environments for their tectonic settings. Both groups were probably generated in arc to back arc environment during the reworking of Saharan Metacraton through subduction-accretion-collision in Sudan at the end of Mesoproterozoic and beginning of the Neoproterozoic at ~1.0 Ga, coevally with the assemblage of Rodinia Supercontinent.

Acknowledgment

We are thankfulness to Professor Chen Nengsong, Professor Ma and Dr. Wang Liangxun for their financial support to our project.

References

1. Abdalla OAE. Ground Water Hydrology of the west-Central Sudan, Hydrochemical and Isotopic Investigations Flow Similuuation and Resources Management, Verlag Dr. Koster Berlin. 1999.
2. Abdel Mageed A. Sudan Industrial Minerals and Rocks, Center for Strategic Studies, Khartoum, Sudan. 1998.
3. Abdel Rahman, E.M., 1993. Geochemical and geotectonic controls of the metallogenic evolution of selected ophiolite complexes from the Sudan. Berl. Geowiss. Abh., A 145 (175 pp).
4. Abdel Rahman, E.M., Harms, U., Schandelmeier, H., Franz, G., Darbyshire, D.P.F., Horn, P., and Muller-Sohnius. 1990. A new ophiolite occurrence in NW Sudan - constraint on Late Proterozoic tectonism-Terra Nova, Melbourne-Oxford- London-Paris.2, 363-376.
5. Abdelsalam, M. G., Liégeois, J. P., and Stern, R. J. 2002. The Saharan Metacraton: Journal of African Earth Sciences, 34, 119-136.
6. Abdelsalam, M. G., Stern, R.J 1996a. Deformational history of the Neoproterozoic Keraf Zone in NE Sudan revealed by Shuttle Imaging Radar. Journal of Geology, 103, 475-491.
7. Abdelsalam, M.G. and Stern, R.J. 1996b. Mapping Precambrian structures in the Sahara Desert with SIR-C/X-SAR radar: The Neoproterozoic Keraf Suture, NE Sudan. Journal of Geophysical Research. 101(10), 065-076.
8. Abdelsalam, M.G., Stern, R.J., Copeland, P., Elfaki, E., Elhur, B., Ibrahim, F.M. 1998. The Neoproterozoic Keraf suture in NE Sudan: sinistral transpression along the eastern margin of west Gondwana. J. Geol., 106, 2: 133-148.
9. Abdelsalam, M.G., Dawoud, A.S., 1991. The Kabus ophiolitic melange, Sudan, and its bearing on the W boundary of the Nubian Shield. J. Geol. Soc. London 148, 83-92.
10. Ahijado, A., Casillas, R., Hernandez-Pacheco, A., 2001. The dyke swarms of the Amanay Massif, Fuerteventura, Canary Islands (Spain). Journal of Asian Earth Sciences 19, 333-345.
11. Ahmed-Said, Y. and Leake, B.E., 1997. The petrogenesis of the Edough amphibolites, Annaba, NE Algeria: two unrelated basic magmas and the lherzolite-harzburgite residue of a possible magma source. Mineralogy and Petrology 59, 207-237.
12. Al Biely, A., I., Farwa, A. G. and Gism ElSid, N. E. 1986. A Geological ,Geophysical and Hydrogeological Investigation In North Kordofan , Department of Geology, University of Khartoum, Khartoum ,Sudan.
13. Aldanmaz, E., Köprübasi, N., Gürer, ÖF, Kaymakci, N., Gourgaud, A. 2006. Geochemical constraints of the Cenozoic, OIB-type alkaline volcanics rocks of NW Turkey: implications for mantle sources and melting processes. Lithos. 86, 50-76.
14. Cabanis, B., Lecolle, M. 1989. Le diagramme La/10-Y/15-Nb: un outil pour la discrimination des series volcaniques et la mise en evidence des processus de me´lange et/ou de contamination crustale. CR

Acad Sci Ser II 309, 2023-2029.
15. Cullers, R.L., Yeh, L.T., Choudhuri, S., Guidotti, C.V., 1974. Rare earth elements in Silurian schists from N.W. Maine. Geochemistry Geosystems Acta 38, 389-400.
16. El Ageed, A.I and Elrabaa, S.M.E., 1981. The Geology and Structural Evolution of The Northeastern Nuba Mountain Kordofan Province, Sudan, Bulletin No 32, Ministry of Energy and Mining Geology and Mineral Resources Department, Sudan.
17. El Gaby, S. 1988/ The Pan-African Belt of Northeast Africa and Adjacent Areas. (Eds) Rein hard O. Greiling.
18. El Khidir, S.O.H. 1997. Metamorphic Evolution of Sodari-Umm Badr Area -North Kordofan, Sudan. (unpublished M.Sc. Thesis) University of Khartoum.
19. Escuder, V.J., Pe´rez-Estau´n, A., Weis, D. 2009. Geochemical constraints on the origin of the late Jurassic proto-Caribbean oceanic crust in Hispaniola. International Journal of Earth Science. 98, 407-425.
20. Ernst, R.E., Bleeker, W., Söderlund, U., Kerr, A.C., 2013. Large Igneous Provinces and supercontinents: Toward completing the plate tectonic revolution, Lithos 174, 1-14.
21. Ernst, R.E., Wingate, M.T.D., Buchan, K.L., Li, Z.X., 2008. Global record of 1600-700 Ma Large Igneous Provinces (LIPs): implications for the reconstruction of the proposed Nuna (Columbia) and Rodinia supercontinents. Precambrian Research 160,159-178.
22. Ernst, R.E., Buchan, K.L., 2001. Large mafic magmatic events through time and links to mantle plume heads. In: Ernst, R.E., Buchan, K.L. (Eds.), Mantle Plumes: Their Identification through Time. Special Paper Geological Society of America 352, 483-575.
23. Ernst, R.E., Buchan, K.L., 1997. Giant radiating dyke swarms: their use in identifying pre-Mesozoic large igneous provinces and mantle plumes. In: Mahoney, J.J., Coffin, M.E. (Eds.), Large Igneous Provinces: Continental, Oceanic, and Planetary Flood Volcanism. Geophysical Monograph, vol. 100, pp. 297-333.
24. Ernst, R.E., Head, J.W., Parfitt, E., Grosfils, E., Wilson, L., 1995. Giant radiating dyke swarms on Earth and Venus. Earth-Science Review 39, 1-58.
25. Evuk, D. O. O., 2013. Geodynamic evolution of the central-eastern Bayuda Desert Basement, Sudan: Structural, petrological, geochemical and geochronological investigations. Ph.D Thesis Technischen University, Berlin.
26. Fitton, J.G. 2007. The OIB paradox. In: Foulger GR, Jurdy DM (eds) Plates, plumes and planetary processes. Geol Soc Amer Spec Pap 430, 387-412.
27. Floyd, P.A., Winchester, I.A. 1978. Identification and discrimination of altered and metamorphosed volcanic rocks using immobile elements. Chemical Geology. 21, 91-306.
28. Floyd, P.A., Winchester, I.A. 1983. Element mobility associated with meta-shear zones within the Ben Hope amphibolite suite, Scotland. Chemical Geology. 39, 1-15.
29. Foster, B.D.F. 1994. Origin and Tectonic Significance of Peninsular Ranges Amphibolites, Ph.D. thesis Faculty of San Diego State University (unpublished).
30. Francalanci, L., Tommasini, S., Conticelli, S., Davies, G. R., 1999. Sr isotope evidence for short magma residence time for the 20th century activity at Stromboli volcano. Italy. Earth and Planetary Science Letters 167, 61 - 69.
31. Frey, F. A., Green, D. H., Roy, S. D. 1978. Integrated models of basalt petrogenesis: a study of quartz tholeiites to olivine melilitites from SE Australia utilizing geochemical and experimental petrological data. Journal of Petrology. 19, 463-513.
32. Gass, I.G. 1981. Pan-African (Late-Proterozoic) plate tectonics of Arabian-Nubian Shield. In: Precambrian plate tectonics (edited by Kroner, A.), Amsterdam, 357-405.
33. Geofrik, 2013. Supercontinente Kenorland (http://geofrik.com/2013/05/06/supercontinente-kenorland/). 2013 publications.
34. Gill, R. 2010. Igneous Rocks and Processes a practical guide. A John Wilery & sons, Ltd, Publication. Malaysia.
35. Goldberg, A.S., 2010. Dyke swarms as indicators of major extensional events in the 1.9-1.2 Ga Columbia supercontinent. Journal of Geodynamics 50, 176-190.
36. Gurenko, A. A., Sobolev, A. V., Hoernle, K., A., Hauff, F., Schmincke, H.,U. 2009. Enriched, HIMU-type peridotite and depleted recycled pyroxenite in the Canary plume: A mixed-up mantle. Earth Planetary Science Letter. 277, 514-524.
37. Gust, D., Arculus, R.J., Kersting, A.B., 1997. Aspects of Magma Sources and Processes in the Honshu Arc. The Canadian Mineralogist 35, 347-365.
38. Halla, J., M.I., Kapyaho, Kurhila, M.I., A.,Lauri, L.S., Nironen M., Ramo, O.T., Sorjonen-Ward, P., & Aikas, O. (2005). “Eurogranites 2005 — Proterozoic and Archean Granites and Related Rocks of the Finnish Precambrian
39. Harms, U., Darbyshire, D.P.F., Denkler, T., Hengst, M. and Schandelmeier, H. 1994. Evolution of the Neoproterozoic Delgo Suture Zone and crustal growth in northern Sudan: geochemical and radiogenic isotope constrains. Geologische Rundsch. 83, 591-603.

40. Harms, U., Schandelmeier, H., Darbyshire, D.P.F., 1990. Pan-African reworked early/ middle Proterozoic crust in NE Africa W of the Nile: Sr and Nd isotope evidence. J. Geol. Soc. London 147, 859-872.
41. Herzberg, C. 2006. Distribution and size of pyroxenite bodies in the mantle. EOS Trans Amer Geophys Union 746:Fall Meeting Supplement, Abstract U12A-04.
42. Herzberg, C., Asimow, P., D. 2008. Petrology of some oceanic island basalts: PRIMELT2. XLS software for primary magma calculation. Geochemistry and Geophysics Geosystem 9, Q09001. doi:10.1029/2008GC002057.
43. Hoffman, P.F., 1997. Tectonic genealogy of North America. In: van der Pluijm, B.A., Marshak, S. (Eds.), Earth structure. An Introduction to Structural Geology and Tectonics. McGraw-Hill, New York, pp. 459-464.
44. Hoffman, P. F., 1991. Did the breakout of Laurentia turn Gondwana inside out? Science, 252, 1409 - 1412.
45. Hollings, P., Kerrich, R. 2004. Geochemical systematics of tholeiites from the 2.86 Ga Pickle Crow Assemblage, northwestern Ontario: arc basalts with positive and negative Nb-Hf anomalies. Precambrian Research, 134, 1-20.
46. Hou, G.T., 2012. Mechanism for three types of mafic dyke swarms. Geoscience Frontiers 3(2), 217-223.
47. Ibinoof, M. A., Bumby, A. J., Grantham, G. H., Abdelrahman, E. M., Eriksson, P. G., le Roux, P. J. 2016. Geology, geochemistry and Sr-Nd constraints of selected metavolcanic rocks from the eastern boundary of the Saharan Metacraton, southern Sudan: A possible revision of the eastern boundary. Precambrian Research, 281, 566-584.
48. Irvine, T.N., Baragar, W.R.A., 1971. A guide to the chemical classification of the common volcanic rocks Can Journal Earth Sciences 8, 523-548.
49. Jagout, E., Palme, H., Baddenhausen, H., Blum, K., Candales, M., Dreibus, G., Spettel, B., Lorenz, V., Wanke, H. 1979. The abundance of major, minor and trace elements in the earth's mantle as derived from primitive ultramafic nodules. Proc 10th Lunar Planet Sci Conf, 2031-2150.
50. Johnson Y. A, Park R. G and Winchester J. A. 1987. Geochemistry, Petrogenesis and Tectonic Significance of the Early Proterozoic Loch Maree Group Amphibolites of the Lewisian Complex, NW Scotland, Geological Society, London, Special Publications. 33, 255-269.
51. Kamber, B.S. 2015. The evolving nature of terrestrial crust from the Hadean, through the Archaean, into the Proterozoic Precambrian Research 258, 48-82.
52. Kelley, K.A., Plank, T., Ludden, J., Staudigel, H., 2003. Composition of altered oceanic crust at ODP Sites 801 and 1149. Geochemistry Geophysics Geosystem 4.
53. Kröner, A. 1985. Ophiolites and evolution of tectonic boundaries in the Late-Proterozoic Arabian-Nubian Shield of NE Africa and Arabia. Precambrian Res., vol. 27, 277-300.
54. Kröner, A., Greilling, R., Reischmann, T., Hussein, I.M., Stern, R.J., Dürr, S., Kruger, J., and Zimmer, M., 1987a. Pan-African crustal evolution in the Nubian segment of the NE Africa, in Kröner, A., (ed.), Proterozoic lithospheric evolution: Am. Geophys. Union Geodynamics series 17, 235-257.
55. Kröner, A., Stern, R.J., Dawoud, A.S., Compston, W., Reischmann, T. 1987 b. The Pan- African continental margin in NE Africa: evidence from the geochronological study of granulites at Sabaloka, Sudan. Earth Planetary Science Letters 85, 91-104.
56. Küster, D., Liégeois, J.P., Matukov, D., Sergeev, S., Lucassen, F., 2008. Zircon geochronology and Sr, Nd, Pb isotope geochemistry of granitoids from Bayuda Desert and Sabaloka (Sudan): evidence for a Bayudian event (920-900 Ma) preceding the Pan-African orogenic cycle (860-590 Ma) at the eastern boundary of the Saharan Metacrat. Precambrian Research. 164, 16-39.
57. Küster, D., Liégeois, J. P. 2001. Sr, Nd isotopes and geochemistry of the Bayuda Desert high-grade metamorphic-basement (Sudan): an early Pan-African oceanic convergent margin, not the edge of the East Saharan ghost craton. Precambrian Research, 109, 1-23.
58. Li, Z. X., Li, X.H., Kinny, P.D., Wang, J. 1999. The Breakup of Rodinia: Did it Start with a Mantle Plume Beneath South China?. Earth Planetary Science Letters. 173 (3), 171-181.
59. Liao, F.X., Zhang, L., Wang Q.Y., Chen, N.S., Santosh, M., Sun, M., Mustafa, H.A., 2014. Geochronology and geochemistry of the dike-swarm garnet-free amphibolites in the Quanji Massif, NW China: Late Paleoproterozoic back arc magmatism and links to amalgamation of the Tarim and North China Cratons and assembly of the Columbia supercontinent. Precambrian Research 249, 33-56.
60. Liu, Y.S., Hu, Z.C., Gao, S., Günther, D., Xu, J., Gao, C.G., Chen, H.H., 2008. In situ analysis of major and trace elements of anhydrous minerals by LA-ICP-MS without applying an internal standard. Chemical Geology 257, 34-43.
61. Ilnicki, S. 2010. Petrogenesis of continental mafic dykes from the Izera Complex, Karkonosze-Izera Block (West Sudetes, SW Poland). International

Journal of Earth Sciences. 99,745-773.
62. Ilnicki, S. 2011. Variscan prograde and contact metamorphism in metabasites from the Sowia Dolina, Karkonosze-Izera massif (SW Poland). Minerals Magazine. 75,185-212.
63. Mayborn, K.R., Lesher, C.E., 2004. Paleoproterozoic mafic dike swarms of northeast Laurentia: products of plumes or ambient mantle?. Earth and Planetary Science Letters 225, 305-317.
64. Mcculloch, M.T., Gamble, J.A., 1991. Geochemical and geodynamical constraints on subduction zone magmatism. Earth and Planetary Science Letters 102, 358-374.
65. McMenamin, M. A. S. & McMenamin, D. L. 1990. The Emergence of animals; The Cambrian Breakthrough. Columbia University Press, New York.
66. Meschede, M. 1986. A method of discriminating between different types of mid-ocean ridge basalts and continental tholeiites with the Nb-Zr-Y diagram.
67. Meert, J.G., 2002. Paleomagnetic evidence for a Paleo-Mesoproterozoic supercontinent Columbia. Gondwana Research 5, 207-216.
68. Mayborn, K.R., Lesher, C.E., 2004. Paleoproterozoic mafic dike swarms of northeast Laurentia: products of plumes or ambient mantle?. Earth and Planetary Science Letters 225, 305-317.
69. Meert, J.G., 2012. What's in a name? The Columbia (Paleopangaea/Nuna) supercontinent. Gondwana Research 21, 987-993.
70. Miyashiro, A., Shido, F., 1975. Tholeiitic and calc-alkalic series in relation to the behaviors of titanium, vanadium, chromium and nickel. American Journal of Science 275, 265-277.
71. Mustafa, H. A., 2007. A concept of the relationship between metamorphism and structures in El Boeid area, North Kordofan State, Sudan. M.Sc. Thesis, University of Kordofan.
72. Mustafa, H. A., Chen, N. S., Wang, L. X., Ma, C. Q., Liao, F. X., Wang, L., Salih, M. A., Abdelsamad, M. A. 2019. Geochronology and geochemistry of the amphibolites from Jebel El Eiza'a, El Obeid area: Insights into the Neoproterozoic tectonic (Rodinia) evolution in Sudan. In preparation.
73. Mustafa, H. A., Chen, N. S., Salih, M. A., Abdelsamad, M. A., Slama, E.M., Wang, L. X., Ma, C. Q., Liao, F. X., Wang, L., 2018c. Geochemistry and Petrogenesis of the amphibolites from Jebel Kordofan - El Obeid Area, North Kordofan, Sudan. African Journal of Geosciences. 1, 40-59.Nance, R.D., Murphy, J.B., Santosh, M., 2014. The supercontinent cycle: a retrospective essay. Gondwana Research 25, 4-29.
74. Orville, P.M., 1969. A model for metamorphic differentiation of thin layered amphibolites: American Journal of Science. 64-86.
75. Pearce, J.A., 1996. A user's guide to basalt discrimination diagrams. In: Wyman, D.A. (ed.), Trace Element Geochemistry of Volcanic Rocks: Applications for Massive Sulfide Exploration. Geological Association of Canada, Short Course Notes. 12, 79-113.
76. Pearce, J. A., Peate, D. W. 1995. Tectonic implications of the composition of volcanic arc magmas. Ann Review Earth Planetary Science. 23, 251-285.
77. Pearce, J.A., Nigel, B. W., Harris and Andrew, G. Trindle. 1984. Trace Element Discrimination Diagrams for the Tectonic Interpretation of Granitic Rocks. Department of Earth Sciences, The Open University, Milton Keynes, MK76AA, Bucks, England.
78. Pearce, J.A., Norry, M.J. 1979. Petrogenetic implications of Ti, Zr, Yand Nb variations in volcanic rocks. Contribution of Mineral Petrology 69, 33-47.
79. Peng, P., Zhai, M.G., Guo, J.H., Kusky, T., Zhao, T.P., 2007. Nature of mantle source contributions and crystal differentiation in the petrogenesis of the 1.78 Ga mafic dykes in the central North China craton. Gondwana Research 12, 29-46.
80. Pesonen, L.J., Salminen, J., Veikkolainen, T. 2012. International Project "Supercontinent Symposium" [. Kumpula Campus, University of Helsinki.
81. Powell, C. M., Li, Z. X., McElhinny, M. W., Meert, J. G., Park, J. K. 1993. Paleomagnetic constraints on timing of the Neoproterozoic break-up of Rodinia and the Cambrian formation of Gondwana. Geology, 21, 889-892.
82. Reddy, S.M., Evans, D.A.D., 2009. Palaeoproterozoic supercontinents and global evolution: correlations from core to atmosphere. Special Publication Geological Society, 323, 1-26.
83. Ries, A.C., Shackleton, R.M., Dawoud, A.S. 1985. Geochronology, geochemistry and tectonics of the NE Bayuda Desert in northern Sudan: Implication for the western margin of the late Proterozoic fold belt of NE Africa. Precambrian Research 30, 43-62.
84. Roberts, N.M.W., 2013. The boring billion? - Lid tectonics, continental growth and Environmental change associated with the Columbia supercontinent. Geoscience Frontiers 4, 681-691.
85. Rollinson, H.R., 1993. Using geochemical data: Evaluation, Presentation, Interpretation. Longman, New York, 352pp.
86. Rodis, H.J, Hassan, A and Wahadan, L. 1964. Ground Water Geology of Kordofan Province Bulletin No. 14, Ministry of Mineral Resources, Geological Survey Department, Khartoum, Sudan.
87. Rogers, J.J.W., 1996. A history of continents in the past three billion years. J. Geology 104, 91-107.

88. Rogers, J.J.W., Santosh, M., 2002. Configuration of Columbia, a Mesoproterozoic supercontinent. Gondwana Research 5, 5-22.
89. Rogers, J.J.W., Santosh, M., 2003. Supercontinents in Earth History. Gondwana Research 6, 357-368.
90. Rogers, J.J.W., 2012. Did natural fission of 235U in the earth lead to formation of the supercontinent Columbia? Geoscience Frontiers 3, 369-374.
91. Rollinson, H.R., 1993. Using geochemical data: Evaluation, Presentation, Interpretation. Longman, New York, 352pp.
92. Williams, H., Hoffman, P. H., Lewry, J. F., Monger, J.W.H. & Rivers, T. 1991. Anatomy of North America: thematic geologic portrayals of the continents. Tectonophysics, 187, 117-134.
93. Schandelmeier, H., Wipfler, E., Küster, D., Sultan, M., Becker, R., Stern, R.J., Abdelsalam, M.G. 1994. Atmur Delgo suture: A Neoproterozoic oceanic basin extending into the interior of northeast Africa. Geology 22, 563-566.
94. Schandelmeier, H., Richter, A., Harms, U., Abdel Rahman, E.M. 1990. Lithology and structure of the late Proterozoic Jebel Rahib fold-and-thrust belt (SW Sudan). Berliner Geowissen Abher (A) 120. 1, 15-30.
95. Schandelmeier, H., Darbyshire, D.P.F., Harms, U., Richter, A. 1988. The E Saharan Craton: evidence for pre-Pan-African crust in NE Africa W of the Nile. In: El Gaby, S., Greiling, R.O. (Eds.). The Pan-Africa belts in NE Africa and Adjacent areas. Friedr. Vieweg and Sohn.. 69-94.
96. Schandelmeier, H., Richter, A., Harms, U. 1987. Proterozoic deformation of the East Saharan Craton in southeast Libya, South Egypt and North Sudan. Tectono Physics 140, 233-246.
97. Staudigel, H., Davies, G.R., Hart, S.R., Marchant, K.M., Smith, B.M., 1995. Large scale isotopic Sr, Nd and O isotopic anatomy of altered oceanic crust: DSDP/ODP sites 417/ 418. Earth and Planetary Science Letters 130, 169-185.
98. Stein, M. and Hofmann, A.W. 1994. Mantle plumes and episodic crustal growth. Nature 372, 63-68.
99. Stern, R.J. 1994. Arc assembly and continental collision in the Neoproterozoic East African Orogen; implication for the consolidation of Gondwanaland. Annual Reviews of Earth and Planetary Science 22, 319-351.
100. Stern, R.J. and Dawoud, A.S. 1991. Late Precambrian (740Ma) Charnokite, Enderbite, and granite from Jebel Moya, Sudan: a link between the Mozambique Belt and the Arabian- Nubian Shield? Journal of Geology. 99, 648-659.
101. Stern, R.J., Kröner, A., Manton, W.I., Reischmann, T., Mansour, M., Hussein, I.M. 1989. Geochronology of the late Precambrian Hamisana shear zone, Red Sea Hills, Sudan and Egypt. Journal of Geological Society, London, 146, 1017-1029.
102. Stow, H., Neilson, M.J., Neathery, T.L., 1984 Petrography, Geochemistry, and Tectonic Significance of the Amphibolites of the Alabama Piedmont. American Journal of Science, 284, (416-436).
103. Sun, S.S., McDonough, W.F., 1989. Chemical and isotopic systematics of oceanic basalt: implications for mantle composition and processes. In Sanders, A.D., Norry, M.J. (eds.), Magmatism in the Ocean Basins. Geological Society. Special Publication, London 42, 313-345.
104. Sun, S., Nesbitt, R.V. 1978. Geochemical regularities and genetic significance of ophiolitic basalts: Geology 6, (689-693).
105. Turner, F.J., and Verhoogen, J., 1960, Igneous and metamorphic petrology: McGraw-Hill, New York, p 694.
106. Vail, J.R., 1990. Geochronology of the Sudan. Overseas Geology and Mineral Resources, vol. 66.
107. Vail, J.R. 1978. Outline of the geology and mineral deposits of the Democratic Republic of the Sudan and adjacent areas. Overseas Geology and Mineral Resources, 49, 67 pp., London.
108. Vail, J.R., 1973. Outline of the Geology of the Nuba Mountains and Vicinity Southern Kordofan Province, Sudan, vol. 23. Bulletin of the Geological and Mineral Resources Authority of the Sudan.
109. Vail, J.R. 1972. Geological reconnaissance in the Zalingei and Jebel Marra areas of western Darfur Province. Sudan Geological Survey Department Bulletin 14, 50 p.
110. Vail, J.R., 1971. Geological reconnaissance in part of Berber District, Northern Province, Sudan: Sudan Geol. Survey Department Bulletin. 18, 76.
111. Walker, K.B., Joplin, G.A., Lovering, J.F. and Green, R., 1960. Metamorphic and metasomatic convergence of basic igneous rocks and lime-magnesia sediments of the Precambrian of northwestern Queensland. Geological Society of Australia. 6, 149-178.
112. Weaver, B.L., Tarney, J., 1981. Empirical approach to estimating the composition of the continental crust. Nature, 310, 575-577.
113. Weil, A. B., Van der Voo R., Niocaill, M. C., Meert, J. G., 1998. The Proterozoic supercontinent Rodinia: paleomagnetically derived reconstructions for 1100 to 800 Ma. Earth and Planetary Science Letters 154, 13-24.
114. Wingate, M. T. D. & Giddings, J. W.2000. Age and Palaeomaganetism of the mundine well dyke swarm, western Austaralia: implications for an Australia - Laurentia connection at 755 Ma. Precambrian

Research, 100, 335 - 357.
115. Wingate, M. T. D., Campbell, I.H., Compston, W., Gibson, G. M. 1998 Ion Microprobe U-Pb Ages for Neoproterozoic Basaltic Magmatism in South-Central Australia and Implications for the Breakup of Rodinia. Precambrian Research, 87, 135-159.
116. Wilson, M.1993. Igneous petrogenesis: a global tectonic approach. Chapman and Hall, London 466 p.
117. Winchester, J. A., Floyd, P. A., 1977. Geochemical discrimination of different magma series and their differentiation products using immobile elements. Chemical Geology, 20, 325-343.
118. Wood, D.A., Tamey, J., Weaver, B.L. 1981. Trace element variations in Atlantic Ocean basalts and Proterozoic dykes from Northwest Scotland: their bearing upon the nature and geochemical evolution of the upper mantle. Tectonophysics. 75, 91-112
119. Wood, D. A., 1980. The application of a Th-Hf-Ta diagram to problems of tectono- magmatic classification and to establishing the nature of crustal contamination of basaltic lavas of the British Tertiary volcanic province. Earth and Planetary Science Letters. 50, 11-30.
120. Yang, Q. Y., Santosh, M. 2014. Late Paleoproterozoic post-collisional magmatism in the North China Craton: Geochemistry, zircon U-Pb geochronology and Hf isotope of the pyroxenite-gabbro-diorite suite from Xinghe, Inner Mongolia. International Geology Review.
121. Zhang, C.L., Li, Z.X., Li, X.H., Ye, H.M., 2009. Neoproterozoic mafic dyke swarms at the northern margin of the Tarim Block. NW China: age, geochemistry, petrogenesis and tectonic implications. Journal of Asian Earth Science 35, 167-179.
122. Zhao, G.C., Cawood, P.A., Wilde, S.A., Sun, M., 2002a. Review of global 2.1-1.8 Ga orogens: implications for a pre-Rodinia supercontinent. Earth-Science Review 59, 125-162.
123. Zhao, G.C., Wilde, S.A., Cawood, P.A., Sun, M., 2002b. SHRIMP U-Pb zircon ages of the Fuping Complex: implications for accretion and assembly of the North China Craton. American Journal of Science 302, 191-226.
124. Zhao, G.C., Cawood, P.A., Wilde, S.A., et al., 2002c. Review of global 2.1-1.8 Ga orogens: implications for a pre-Rodinia supercontinent. Earth Science Review, 59: 125-162.
125. Zhao, G.C., Sun, M., Wilde, S.A., 2003. Assembly, Accretion and Breakup of the Paleo-Mesoproterozoic Columbia Supercontinent: Records in the North China Craton. Gondwana Research 6, 417-434.
126. Zhao, G.C., Sun, M., Wilde, S.A., Li, S.Z., 2004. A Paleo-Mesoproterozoic supercontinent: assembly, growth and breakup. Earth-Science Review 67, 91-123.
127. Zhao, G.C., Li, S.Z., Sun, M., Wilde, S.A. 2011. Assembly, accretion, and break-up of the Palaeo-Mesoproterozoic Columbia supercontinent: record in the North China Craton revisited. International Geology Review. 53, 1331-1356.